EVOLUTION

Two-stage evolution of mammalian adipose tissue thermogenesis

Susanne Keipert[1]†, Michael J. Gaudry[1]†, Maria Kutschke[1], Michaela Keuper[1], Margeoux A. S. Dela Rosa[2], Yiming Cheng[3,4,5], José M. Monroy Kuhn[6], Rutger Laterveer[1], Camila A. Cotrim[2], Peter Giere[7], Fabiana Perocchi[3,4,5], Regina Feederle[8], Paul G. Crichton[2], Dominik Lutter[6], Martin Jastroch[1]*

Brown adipose tissue (BAT) is a heater organ that expresses thermogenic uncoupling protein 1 (UCP1) to maintain high body temperatures during cold stress. BAT thermogenesis is considered an overarching mammalian trait, but its evolutionary origin is unknown. We show that adipose tissue of marsupials, which diverged from eutherian mammals ~150 million years ago, expresses a nonthermogenic UCP1 variant governed by a partial transcriptomic BAT signature similar to that found in eutherian beige adipose tissue. We found that the reconstructed UCP1 sequence of the common eutherian ancestor displayed typical thermogenic activity, whereas therian ancestor UCP1 is nonthermogenic. Thus, mammalian adipose tissue thermogenesis may have evolved in two distinct stages, with a prethermogenic stage in the common therian ancestor linking UCP1 expression to adipose tissue and thermal stress. We propose that in a second stage, UCP1 acquired its thermogenic function specifically in eutherians, such that the onset of mammalian BAT thermogenesis occurred only after the divergence from marsupials.

The evolution of thermogenesis in mammals supported the maintenance of high body temperatures, which came with the benefits of climate-independent motility and reproduction, increased brain size, and regulation of growth and body weight. In particular, brown adipose tissue (BAT), the main organ for nonshivering thermogenesis in mammals, enables newborns, small-sized species, and hibernators to increase heat output to overcome cold stress. Critical for BAT thermogenesis is the expression of uncoupling protein 1 (UCP1), which resides in the inner mitochondrial membrane. Free fatty acids, liberated by cold- or diet-stimulated lipolysis, induce proton transport by UCP1 to uncouple the respiratory chain from adenosine triphosphate (ATP) production to accelerate metabolism and release more chemical energy as heat (*1*). Although BAT has been labeled a "mammalian prerogative" (*2*), experimental studies on BAT and UCP1 function are limited to only a few eutherian species, mostly rodents and humans. Specifically, investigations in humans have been fostered by the identification of functional BAT in adults (*3*–*5*), which represents a promising therapeutic target to combat metabolic diseases such as obesity and cardiovascular complications by increasing energy metabolism (*6*). In white adipose tissue (WAT) of mice and humans, cells with partial BAT features, called beige adipocytes, can emerge under stress conditions, but their physiological role is still a matter of debate (*7*, *8*). Pharmacologic and genetic manipulations in mice have been used to understand how BAT thermogenesis can be activated, brown adipocytes recruited, or white adipocytes transformed into beige cells. The structure of human UCP1 has been determined (*9*, *10*), but the mechanism of proton transport, which is pivotal for thermogenesis, has remained enigmatic.

As revealed by comparative genomics, the *Ucp1* gene is ancient, dating back to the divergence of teleosts (ray-finned fish) and sarcopterygians (lobe-finned fish) about 420 million years ago (*11*). In fish, *Ucp1* is expressed in liver and brain tissues but not in adipocytes, raising questions surrounding the evolutionary timing of targeted *Ucp1* expression in adipocyte-like cells, as in mice and humans. Furthermore, the protein function of the fish UCP1 ortholog is unknown, and phylogenetic inference shows its sequence to be quite similar to that of its paralogs UCP2 and UCP3. Apart from mammalian UCP1 variants, all other members of the mitochondrial solute carrier family SLC25 are metabolite transporters (*12*, *13*). Even UCP2 and UCP3, previously thought to be alternative thermogenic protonophores, have no physiological role in thermogenesis (*14*) but appear to transport small metabolites (*12*). The demonstration of BAT thermogenesis in an afrotherian species, the lesser hedgehog tenrec (*Echinops telfairi*), revealed that UCP1 acquired its heat-producing role before the divergence of afrotherian and boreoeutherian mammals, about 80 million years ago (*15*). The role of UCP1 in marsupials, which diverged from eutherians about 120 million to 180 million years ago, is less clear. Marsupials possess a *Ucp1* ortholog (*16*), but in vivo evidence for adaptive nonshivering thermogenesis has remained equivocal (*17*).

We discovered a gene expression signature of *Ucp1*-expressing adipose tissue (AT) in marsupials using global transcriptomic methods that is reminiscent of eutherian beige adipose tissue. We then assessed the thermogenic capacity of marsupial UCP1 and resurrected the reconstructed *Ucp1* sequence of the common eutherian and therian ancestors for functional analyses to pinpoint the origin of UCP1-dependent thermogenesis.

Results

Development of endothermy and Ucp1 expression in the opossum

To compare the transcriptomes of marsupial and eutherian AT, we scrutinized the short-tailed opossum, *Monodelphis domestica*, a marsupial model organism with high genomic sequencing coverage. Offspring of *M. domestica* develop predominantly ex utero and are hairless and initially ectothermic, receiving body heat from the mother (Fig. 1A). The young were investigated during and shortly after weaning at ages of 6 to 13 weeks, at which point they experience thermal stress, and during adulthood at 33 weeks (Fig. 1B). Body weight, length, blood markers, and the appearance of AT were recorded during development (Fig. 1, C and D, and fig. S1). Infrared thermography of eye temperatures revealed that 6-week-old juveniles separated from their mothers were unable to maintain the nursing temperature of about 32°C, in contrast to the sustained endothermic homeothermy of ≥8-week-old individuals (Fig. 1E). Body temperatures were confirmed by rectal probing (Fig. 1F) and were consistent with reports on the development of thermoregulatory competence in marsupials (*18*, *19*). *Ucp1* mRNA expression was exclusively found in AT depots (Fig. 1G), with amounts transiently increasing from age 6 weeks to 10 weeks (Fig. 1H), coinciding with the onset of sustained endothermy. *Ucp1* mRNA expression was lower in the interscapular AT, the canonical location of eutherian BAT, than in the inguinal AT, which is a prominent site for the occurrence of beige adipocytes in eutherian mammals. In the anterior subcutaneous AT, *Ucp1* mRNA was barely detectable throughout juvenile development (Fig. 1H).

Comparative transcriptomics reveals a partial browning signature in the opossum

We attempted to understand the underlying molecular network governing marsupial *UCP1*

[1]Department of Molecular Biosciences, The Wenner-Gren Institute, Stockholm University, SE-106 91 Stockholm, Sweden. [2]Biomedical Research Centre, Norwich Medical School, University of East Anglia, Norwich Research Park, Norwich NR4 7TJ, UK. [3]Institute of Neuronal Cell Biology, Technical University of Munich, 80802 Munich, Germany. [4]Munich Cluster of Systems Neurology, 81377 Munich, Germany. [5]Institute for Diabetes and Obesity (IDO), Helmholtz Zentrum München, 85764 Munich, Germany. [6]Computational Discovery Research, Institute for Diabetes and Obesity (IDO), Helmholtz Diabetes Center (HDC), Helmholtz Zentrum Munich, German Research Center for Environmental Health, German Center for Diabetes Research (DZD), 85764 Neuherberg, Germany. [7]Museum für Naturkunde–Leibniz Institute for Evolution and Biodiversity Science, 10115 Berlin, Germany. [8]Monoclonal Antibody Core Facility, Helmholtz Zentrum München, German Research Center for Environmental Health, 85764 Neuherberg, Germany.
*Corresponding author. Email: martin.jastroch@su.se
†These authors contributed equally to this work.

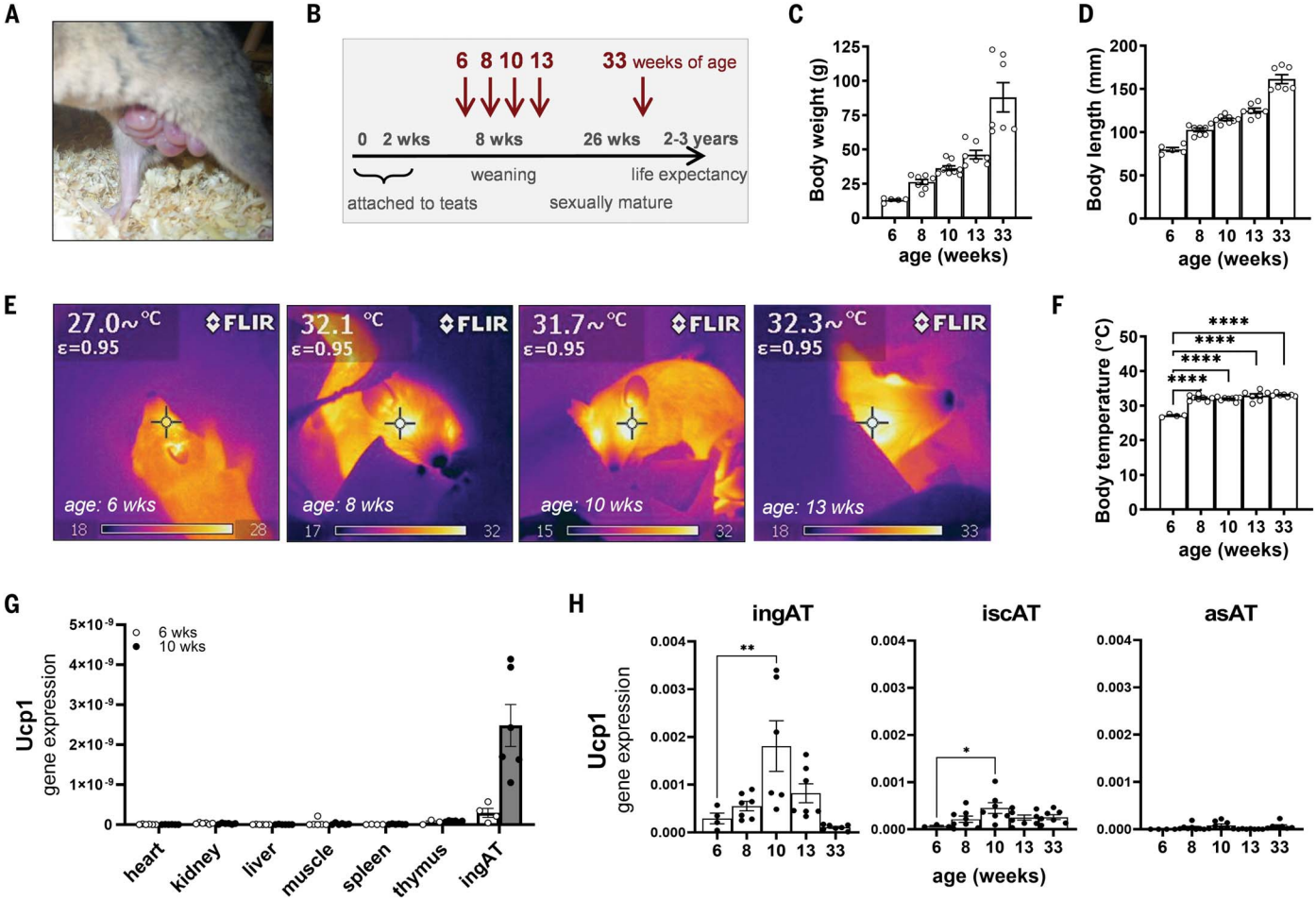

Fig. 1. Development of sustained endothermy and *Ucp1* expression in the juvenile opossum (*M. domestica*). (**A**) Juveniles are born immature and attach to the teats. (**B**) Overview of age and tissue sampling. (**C**) Body weights. (**D**) Body length. (**E**) Infrared imaging of eye temperatures shown after separation from the mother. FLIR, forward-looking infrared. (**F**) Rectal body temperatures measured immediately postmortem. (**G**) Detection of *Ucp1* mRNA with quantitative polymerase chain reaction in multiple tissues. ingAT, inguinal adipose tissue. (**H**) Longitudinal analysis of *Ucp1* mRNA in adipose tissue depots. iscAT, interscapular adipose tissue; asAT, anterior subcutaneous adipose tissue. Data are mean ± SEM; n = 4 to 9 animals. Statistical significance between groups is denoted by $^{*}P < 0.05$, $^{**}P < 0.01$, $^{****}P < 0.0001$. One-way analysis of variance (ANOVA; Tukey's post hoc test).

expression by determining the global transcriptomic changes of 6-week-old (low *UCP1*) versus 10-week-old (high *UCP1*) opossums. Comparative analyses to cold-induced changes in mouse BAT served to identify common or divergent features between marsupial and eutherian AT. Plotting the whole cold-induced mouse BAT transcriptome (y axis) against the marsupial transcriptome (x axis) depicted common significant gene expression changes (Fig. 2A, purple dots). The overlap or enrichment of these regulated genes (squares) was significantly higher than expected in all intersections between mouse BAT and opossum inguinal AT (all $P < 0.001$) but not between mouse BAT and interscapular AT or anterior subcutaneous AT. Thus, opossum inguinal AT displayed a gene regulation network similar to that in cold-activated mouse BAT. Expression of beta-3 adrenergic receptor (*Adrb3*) mRNA, which predominantly mediates the thermogenic response in eutherian BAT, was increased specifically in opossum inguinal AT, whereas abundance of the beta-1 adrenergic receptor (*Adrb1*) mRNA was increased in all adipose depots (Fig. 2B). Of the potential UCP1-independent thermogenic pathways, the opossum shows increased expression only of creatine kinase B (*Ckb*) (fig. S2A), implicated in an ATP-dependent thermogenic futile creatine cycle (*20*), but no alterations in *Alpl*, *Serca2b*, or any ATP-synthase subunits (fig. S2B). Differentially expressed genes (DEGs) of marsupial inguinal AT between 6-week-old and 10-week-old animals were compared with those of interscapular AT and anterior subcutaneous AT and with mouse BAT and WAT. The heatmap indicates that expression patterns in all AT depots of 6-week-old opossums resemble those in mouse WAT (Fig. 2C). A molecular network was observed in marsupial inguinal AT at 10 weeks of age that resembled that of mouse BAT. The mouse BAT–like expression pattern of these genes is less pronounced in interscapular AT and absent in the anterior subcutaneous depot (Fig. 2C). A stringent BAT signature derived from mouse and human transcriptomes was used to approximate the degree of browning from white to beige to brown AT (*21*). The reference mouse transcriptome of BAT exhibited full browning irrespective of acclimation temperature (Fig. 2D), whereas mouse inguinal AT showed a partial browning signature in the cold, characteristic of beige adipocytes with induced *Ucp1* expression (*7*, *22*). The opossum ATs enhance the browning probability alongside increased *Ucp1* expression from 6 to 10 weeks of age, particularly in inguinal AT. However, none of the individuals displayed a pure BAT-specific molecular signature, which is represented by

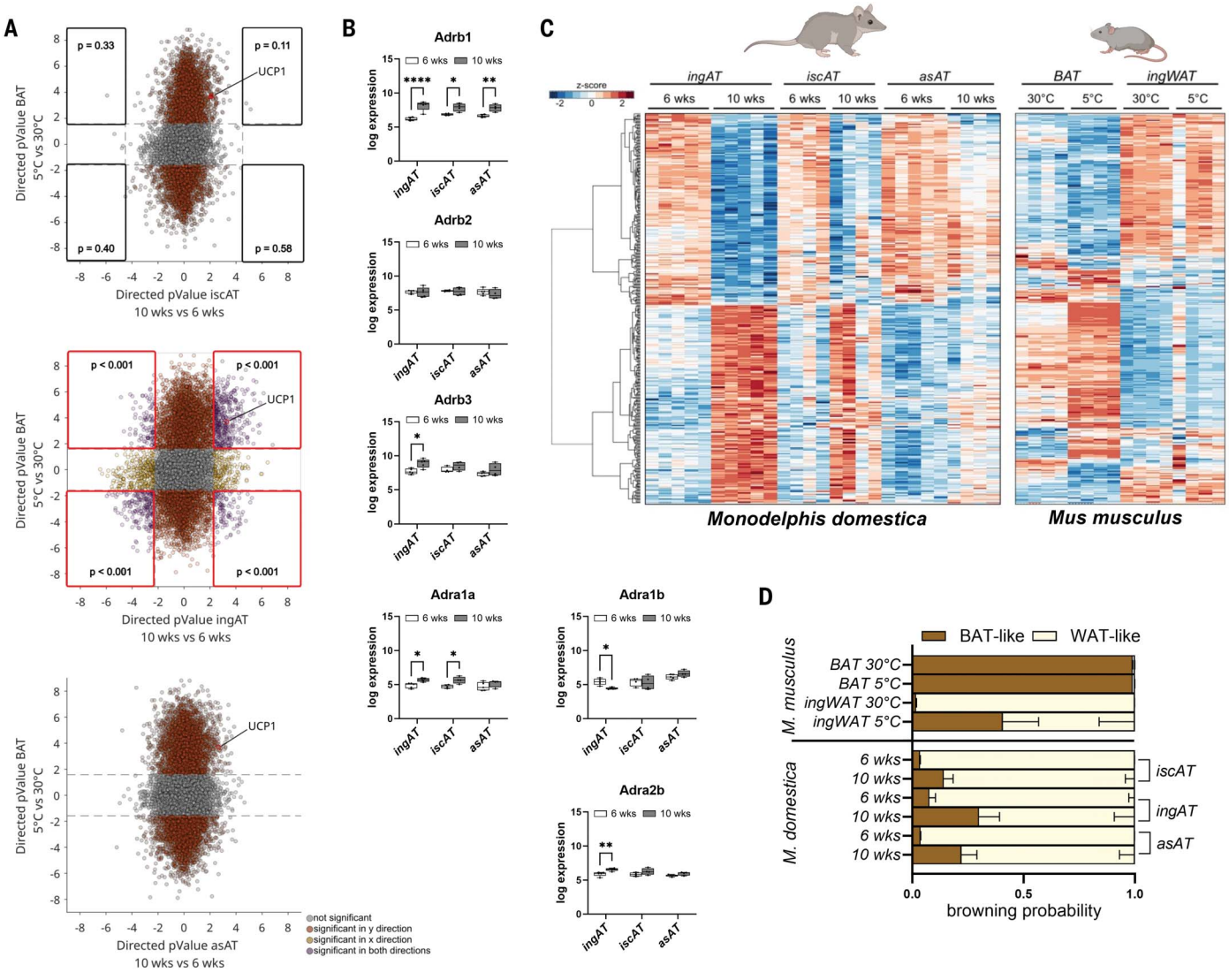

Fig. 2. Comparative analysis of the opossum adipose transcriptome reveals a rudimentary browning signature. (**A**) To show commonly regulated genes in adipose tissue, the directed *P* value of mouse BAT mRNAs (cold versus warm) was plotted against the *P* value of opossum adipose mRNAs (6 weeks old versus 10 weeks old). Interspecies similarities are found in particular in the inguinal AT mRNAs. Significant overlap between mouse and opossum regulated genes passing false discovery rate correction (squares) was estimated using a hypergeometric distribution test. A significant overlap ($P < 0.001$) is indicated in red. (**B**) Regulation of adrenergic receptors in opossum adipose tissue from 6 to 10 weeks of age. Box plots showing the distribution of log gene expression level. The central mark indicates the median, and the bottom and top edges of the box indicate the 25th and 75th percentiles, respectively. The whiskers extend to the most extreme data points. (**C**) Heatmap of cross-species and tissue comparisons of inguinal AT DEGs. (**D**) Browning probability using the ProFAT tool. Data are mean ± SEM; $n = 4$ or 5 animals. (B) Statistical significance between groups is denoted by $^{*}P < 0.05$, $^{**}P < 0.01$, $^{****}P < 0.0001$. Two-way ANOVA (Sidak). Opossum and mouse images in (C) were created with BioRender.com.

a probability of 1.0, depicted as a fully brown bar in Fig. 2D. Thus, marsupial AT appears to regulate *Ucp1* in a molecular network that is reminiscent of that proposed to occur in eutherian beige adipose tissue.

Comparative respirometry demonstrates lack of thermogenic function of marsupial UCP1

We investigated marsupial UCP1 function by overexpressing mouse and opossum UCP1 in human embryonic kidney (HEK) 293 cells, an established mammalian test system (*23*, *24*) (Fig. 3A). *Ucp1* mRNA expression was similar between mouse (MmUCP1) and opossum UCP1 (MdUCP1) (fig. S3A). Among commercially available mouse UCP1 antibodies, only one detected opossum UCP1 weakly, prompting us to generate a strong, specific opossum UCP1 antibody and protein standards of mouse and opossum UCP1 for the immunoblot quantification as described previously (*15*) (fig. S3, B and C). Protein standards and the specific antibodies enabled us to quantify the UCP1 protein levels of low and high mouse UCP1–expressing clones (Fig. 3B and fig. S3, D, F, and H) and opossum UCP1–expressing clones (Fig. 3C and fig. S3, E, G, and H). We applied plate-based respirometry of intact HEK293 cells to measure UCP1-dependent proton leak upon stimulation with naturally occurring activators, such as the long-chain fatty acid palmitate and the short-chain fatty acid nonanoic acid, as well as the more recently identified artificial activator arotinoid acid, a retinoic acid analog (commonly referred to as TTNPB) (*25*) (Fig. 3D). Palmitate, TTNPB, and nonanoic acids activated proton leak specifically in cells expressing low or high levels of mouse UCP1 but not in cells expressing high levels of opossum UCP1 or empty vector

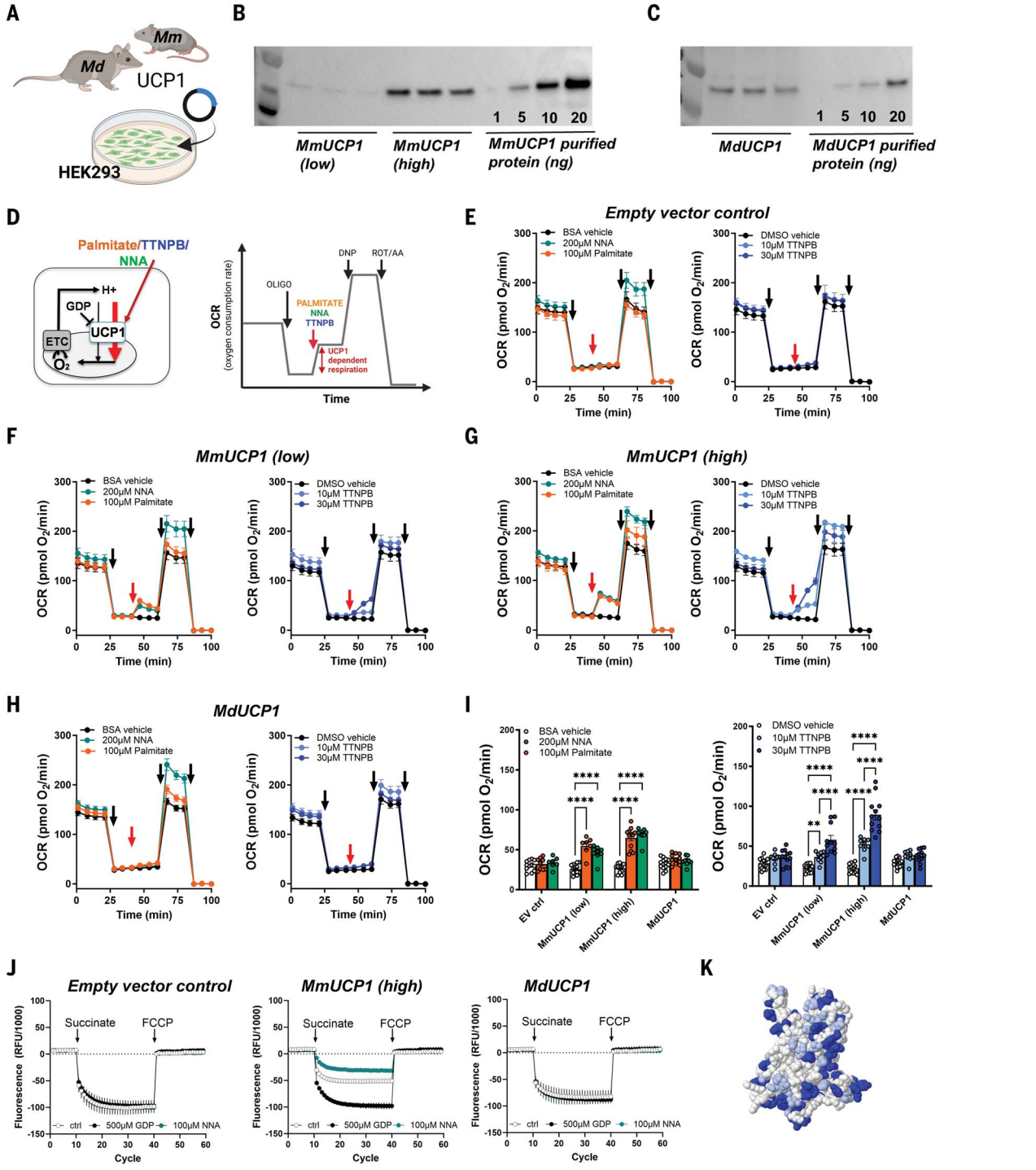

Fig. 3. Comparative respirometry demonstrates lack of thermogenic function of marsupial UCP1. (**A**) Cartoon of reductionist approach expressing UCP1 variants in mammalian cell culture. (**B**) Western blotting of 20 μg of protein lysate from low and high mouse UCP1–expressing HEK293 cells (MmUCP1) and various amounts of mouse UCP1 standard, using the anti-mouse UCP1 antibody. (**C**) Western blotting of 20 μg of protein lysate from opossum UCP1–expressing HEK293 cells (MdUCP1) and various amounts of opossum UCP1 standard, using the anti-opossum UCP1 antibody. (**D**) Scheme of UCP1 regulation and time-lapse respiration measurement to obtain the oxygen consumption rate (OCR). Arrows indicate the injections of oligomycin (OLIGO), UCP1 activator [nonanoic acid (NNA)] or vehicle control, dinitrophenol (DNP), and rotenone and antimycin A (ROT/AA). ETC, electron transport chain; GDP, guanosine diphosphate. (**E** to **H**) Aggregated respiration traces using NNA, palmitate, or TTNPB as specific UCP1 activators. The red arrow indicates the injection of activator or vehicle in wells with empty vector control, mouse (MmUCP1) low or high, and opossum (MdUCP1) expressing HEK293 cells. (**I**) Bar chart of OCR upon activator or vehicle treatment. (**J**) Measurement of mitochondrial membrane potential in isolated mitochondria using safranin O quenching. FCCP, carbonyl cyanide-*p*-trifluoromethoxyphenylhydrazone. (**K**) UCP1 structural model based on threading into the adenine translocase structural model. Identical amino acids in white, similar in light blue, and dissimilar in dark blue. Data are shown as mean ± SEM; (E) to (I): $n = 7$ to 15 measurements on three independent days; (J): $n = 3$ independent experiments. Statistical significance between groups is denoted by $^{**}P < 0.01$, $^{****}P < 0.0001$. (I) Two-way ANOVA (Tukey's post hoc test). (A) and (D) were partially created with BioRender.com.

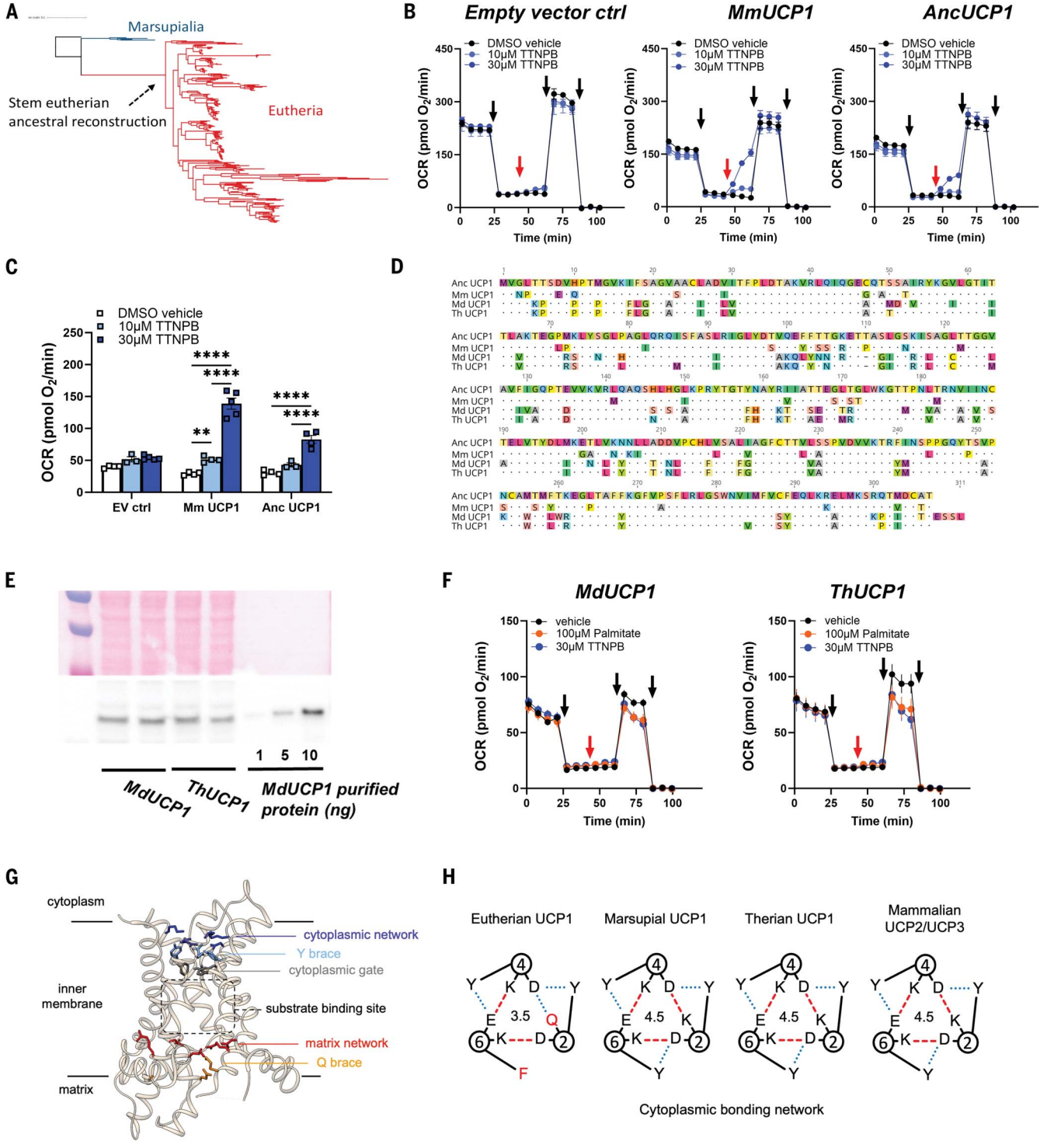

Fig. 4. Construction and functional analysis of stem eutherian and therian ancestor UCP1. (**A**) Phylogenetic tree of UCP1 depicting stem eutherian reconstruction. (**B**) OCR of HEK293 cells expressing the empty vector control, mouse (Mm) UCP1, and reconstructed stem eutherian ancestor (Anc) UCP1. Red arrow indicates the injection of activator (TTNPB) or vehicle. (**C**) Bar chart of OCR upon activator or vehicle treatment. (**D**) Alignment summarizing differences of the stem eutherian ancestor UCP1 (Anc) to mouse UCP1 (Mm), opossum UCP1 (Md), and stem therian ancestor UCP1 (Th). (**E**) Western blotting of 20 μg of protein lysate from transiently transfected HEK293 cells expressing opossum UCP1 (MdUCP1), stem therian ancestor UCP1 (ThUCP1), and various amounts of opossum UCP1 standard, using the anti-opossum UCP1 antibody. (**F**) OCR of HEK293 cells expressing Md or ThUCP1. (**G**) Key mitochondrial carrier structural features [Protein Data Bank ID 6GCI (*30*)]. (**H**) The cytoplasmic bonding network predicted in eutherian UCP1, differing from marsupial UCP1, reconstructed therian UCP1, and mammalian UCP2 and UCP3, which are all identical. Data are shown as mean ± SEM. (B) and (C): n = 3 to 5 measurements per group; (F): n = 8 to 12 measurements per group. Statistical significance between groups is denoted by $^{**}P < 0.01$, $^{****}P < 0.0001$. (C) Two-way ANOVA (Tukey's post hoc test).

controls (Fig. 3, E to I). Additionally, no proton transport activity was found in a nonclonal mixture of transiently transfected opossum UCP1 cells (fig. S3, H and I). In isolated mitochondria, mouse UCP1 was activatable with nonanoic acids and fully inhibitable with its canonical inhibitor, guanosine diphosphate, as judged by decreases in mitochondrial membrane potential measured with the fluorometric indicator safranin O. By contrast, neither basal protonophoric activity nor activation or inhibition was observed for opossum UCP1 (Fig. 3J and fig. S3J). Thus, opossum UCP1 is not thermogenic, and typical thermogenic features must have been either introduced at later evolutionary stages or lost in the opossum lineage. Opossum UCP1 displays 65 dissimilar (dark blue) and 46 similar (light blue) amino acids as compared with mouse UCP1 (Fig. 3K), which may reflect changes during the course of evolution that introduced strictly regulated activation and inhibition of UCP1 for regulation of adaptive thermogenic function.

Reconstruction and functional analysis of the stem eutherian and therian ancestor UCP1

To pinpoint the phylogenetic origin of thermogenic UCP1, we collected and verified 237 intact mammalian UCP1 sequences (table S2), excluding the inactive versions (*26*). We applied a maximum likelihood and phylogenetic approach to reconstruct the predicted ancestral UCP1 sequences of the major nodes of the mammalian phylogenetic tree (fig. S4 and tables S2 and S3), such as UCP1 from the stem eutherian ancestor (Fig. 4A). Next, we synthetized the stem eutherian *Ucp1* coding sequence (fig. S4, node 6), controlled for mRNA expression and protein levels (fig. S5, A and B), and tested its function (Fig. 4B and fig. S5C). Proton transport activity of the reconstructed ancient eutherian UCP1 protein was activatable with TTNPB (Fig. 4, B and C) and nonanoic acids (fig. S5C), as is eutherian UCP1 of extant species. Thus, we proposed that the thermogenic function of eutherian UCP1 may have originated before the radiation of eutherian mammals, which occurred around 65 million to 100 million years ago (*27*, *28*). To exclude that marsupials have specifically lost thermogenic UCP1 function, we transiently transfected the reconstructed stem therian *Ucp1* coding sequence (fig. S4, node 8), which appeared to share more similar amino acid residues with opossum than with the stem eutherian UCP1 (Fig. 4D). Protein levels of opossum and therian UCP1 were similar (Fig. 4E) and comparable to previous experiments (fig. S3H). The therian version was not activatable by palmitate or TTNPB (Fig. 4F), similar to opossum UCP1. Thus, good arguments can be put forward that the acquisition of thermogenic function occurred after the divergence of marsupials. The acquired thermogenic features of eutherian UCP1 appear to reside within amino acid residues that are distinct from the marsupial and reconstructed stem therian UCP1 sequence (Fig. 4D). UCPs are members of the mitochondrial carrier family of solute transporters and conserve key structural features to support function (*29*, *30*) (Fig. 4G and fig. S6). Notably, we identified that the predicted cytoplasmic bonding network of UCP1 that gates access to the central cavity from the cytoplasmic side in all eutherian UCP1 variants is distinct from the stronger network found in UCP1 of all marsupials and monotremes (fig. S7), the reconstructed stem therian UCP1 and mammalian UCP2 and UCP3 (*29*, *30*) (Fig. 4H).

Discussion

The evolutionary origin of thermogenic eutherian BAT has been debated, and molecular clues on the evolutionary events incorporating thermogenesis into adipose tissue have been lacking. Our data demonstrate that thermogenic AT appears to have evolved in two stages, with an initial prethermogenic stage in which *Ucp1* expression occurred in AT and coincided with weaning when juveniles experience cold stress, with pathways under adrenergic stimulation, possibly enabling mobilization of fat stores and other metabolic pathways. In a second stage, we propose that gain of thermogenic function of a mitochondrial transporter, UCP1, enabled the mitochondrial proton transport that is required to convert energy to heat.

BAT-like transcriptional control of marsupial *Ucp1* existed before the divergence of Marsupialia about 120 million to 180 million years ago, given exclusive *Ucp1* mRNA expression in AT, with the highest amounts detected during juvenile development of sustained endothermy, identical to what is found in most eutherians. The presence of a partial BAT transcriptomic signature is more reminiscent of that in eutherian beige than brown adipose tissue. In contrast to eutherian BAT, marsupial proto-BAT or beige adipose tissue appears not to be thermogenic, as indicated by the lack of protonophoric activity of marsupial UCP1.

Like those of many of the ~50 different mitochondrial carriers present in mammals, the molecular function of prethermogenic marsupial UCP1 is unknown. The key structural features important for carrier function are well conserved across the UCP subfamily. However, the important cytoplasmic bonding network, for instance, gating the central cavity from the mitochondrial intermembrane space (*9*, *10*, *31*), is identical between marsupial and therian UCP1, and mammalian UCP2 and UCP3, whereas eutherian UCP1 has distinctions that potentially contribute to its protonophoric activity (Fig. 4H). Other conserved residues—the eutherian UCP1–specific glutamate in position 134, for example—were implicated in proton transport by some (*32*) but not by others (*33*). Given the similarity of marsupial UCP1 to nonthermogenic UCP2 and UCP3 (*14*), a conventional metabolite transport function is the likely function of UCP1 in noneutherians (*12*, *31*).

REFERENCES AND NOTES

1. D. G. Nicholls, R. M. Locke, *Physiol. Rev.* **64**, 1–64 (1984).
2. B. Cannon, J. Nedergaard, *Physiol. Rev.* **84**, 277–359 (2004).
3. A. M. Cypess *et al*., *N. Engl. J. Med.* **360**, 1509–1517 (2009).
4. W. D. van Marken Lichtenbelt *et al*., *N. Engl. J. Med.* **360**, 1500–1508 (2009).
5. K. A. Virtanen *et al*., *N. Engl. J. Med.* **360**, 1518–1525 (2009).
6. T. Becher *et al*., *Nat. Med.* **27**, 58–65 (2021).
7. J. Wu *et al*., *Cell* **150**, 366–376 (2012).
8. S. Keipert, M. Jastroch, *Biochim. Biophys. Acta* **1837**, 1075–1082 (2014).
9. S. A. Jones *et al*., *Sci. Adv.* **9**, eadh4251 (2023).
10. Y. Kang, L. Chen, *Nature* **620**, 226–231 (2023).
11. M. Jastroch, S. Wuertz, W. Kloas, M. Klingenspor, *Physiol. Genomics* **22**, 150–156 (2005).
12. A. Vozza *et al*., *Proc. Natl. Acad. Sci. U.S.A.* **111**, 960–965 (2014).
13. F. Palmieri, *Pflugers Arch.* **447**, 689–709 (2004).
14. J. Nedergaard, B. Cannon, *Exp. Physiol.* **88**, 65–84 (2003).
15. R. Oelkrug *et al*., *Nat. Commun.* **4**, 2140 (2013).
16. M. Jastroch *et al*., *Physiol. Genomics* **32**, 161–169 (2008).
17. M. Jastroch, E. T. Polymeropoulos, M. J. Gaudry, *J. Comp. Physiol. B* **191**, 1085–1095 (2021).
18. P. Morrison, J. H. Petajan, *Physiol. Zool.* **35**, 52–65 (1962).
19. F. Geiser, L. Matwiejczyk, R. V. Baudinette, *Physiol. Zool.* **59**, 220–229 (1986).
20. J. F. Rahbani *et al*., *Nature* **590**, 480–485 (2021).
21. Y. Cheng *et al*., *Cell Rep.* **23**, 3112–3125 (2018).
22. J. M. A. de Jong *et al*., *Nat. Metab.* **1**, 830–843 (2019).
23. M. Jastroch, V. Hirschberg, M. Klingenspor, *Biochim. Biophys. Acta* **1817**, 1660–1670 (2012).
24. M. J. Gaudry, M. Jastroch, *Comp. Biochem. Physiol. B Biochem. Mol. Biol.* **255**, 110613 (2021).
25. P. Tomás *et al*., *Biochim. Biophys. Acta* **1658**, 157–164 (2004).
26. M. J. Gaudry *et al*., *Sci. Adv.* **3**, e1602878 (2017).
27. R. W. Meredith *et al*., *Science* **334**, 521–524 (2011).
28. M. A. O'Leary *et al*., *Science* **339**, 662–667 (2013).
29. J. J. Ruprecht, E. R. S. Kunji, *Trends Biochem. Sci.* **45**, 244–258 (2020).
30. J. J. Ruprecht *et al*., *Cell* **176**, 435–447.e15 (2019).
31. A. J. Robinson, C. Overy, E. R. S. Kunji, *Proc. Natl. Acad. Sci. U.S.A.* **105**, 17766–17771 (2008).
32. J. Jiménez-Jiménez *et al*., *J. Mol. Biol.* **359**, 1010–1022 (2006).
33. M. Klingenberg, K. S. Echtay, M. Bienengraeber, E. Winkler, S. G. Huang, *Int. J. Obes.* **23** (suppl. 6), S24–S29 (1999).

ACKNOWLEDGMENTS

We thank P. Grimm and A. Billepp for care of the *Monodelphis* colony, the late J. Zeller for technical assistance, and T. J. Fyda and C. Spencer for assistance with maximum likelihood ancestral sequence reconstruction. **Funding:** This research was supported by the Novo Nordisk Fonden (grant number 0059646 to M.J.), Vetenskapsrådet (2018-03472, 2022-03136 to M.J.), and the Wenner-Gren Foundation (to M.J.). **Author contributions:** S.K. conceived of the experimental plan, designed research, conducted experiments, interpreted the results, and prepared the figures. M.J.G. designed and conducted experiments, interpreted the results, and prepared figures. M.Ku., M.Ke., M.A.S.D.R., and R.L. performed experiments. D.L., J.M.M.K., and Y.C. performed bioinformatical analyses of RNA sequencing (RNA-seq) data and interpreted the data with S.K., F.P., and M.J. Y.C. and F.P. customized the ProFAT tool for this project. R.F. generated the opossum-specific UCP1 antibody. C.A.C. and P.G.C. performed protein bioinformatic and structural assessment. P.G. designed and performed the animal experiments. M.J. conceived of and directed the project, designed research, conducted experiments, interpreted the results, and wrote the manuscript. All authors discussed the results and edited and revised the manuscript. **Competing interests:** The authors declare that they have no competing financial interests. **Data and materials availability:** All data are available in the main article or the supplementary materials and from the corresponding author upon reasonable request. Source data are provided with this paper. All RNA-seq

data have been deposited into the Gene Expression Omnibus (GEO) under accession numbers GSE224318 (*Monodelphis domestica*) and GSE112582 (*Mus musculus*). Correspondence and requests for materials should be addressed to martin.jastroch@su.se.

SUPPLEMENTARY MATERIALS

science.org/doi/10.1126/science.adg1947
Materials and Methods
Figs. S1 to S7
Tables S1 to S4
References (*34*–*43*)
MDAR Reproducibility Checklist
Appendix S1

Submitted 2 July 2023; accepted 8 April 2024
10.1126/science.adg1947